Pzmit

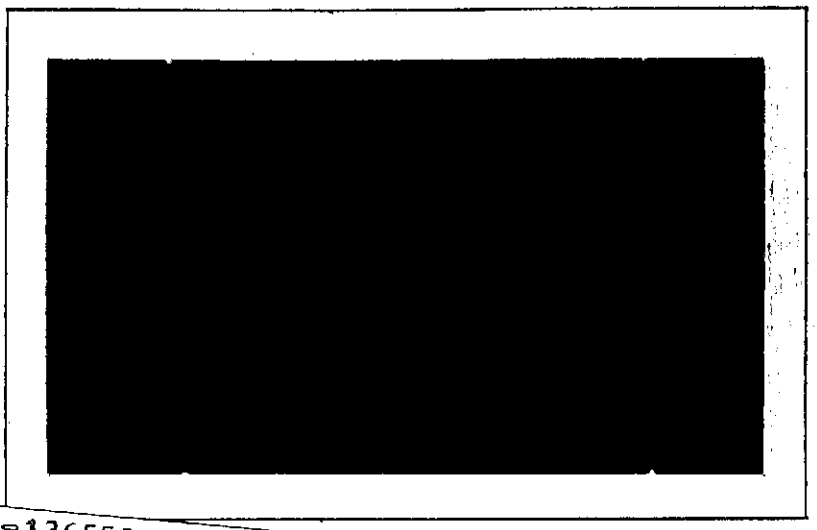

METALS RESEARCH LABORATORY

CARNEGIE INSTITUTE OF TECHNOLOGY

Carnegie-Mellon University

PITTSBURGH, PENNSYLVANIA

National Aeronautics and Space Administration
Research Grant NGR 39-087-047

THE EFFECT OF MICROSTRUCTURE ON THE FRACTURE TOUGHNESS OF TITANIUM ALLOYS

by

R. H. Van Stone and J. R. Low, Jr.

Department of Metallurgy and Materials Science
Carnegie-Mellon University
Pittsburgh, Pennsylvania 15213

NASA Technical Report No. 1-Ti
October 1973

This investigation was made possible by a Research Grant from the National Aeronautics and Space Administration

The high-strength titanium alloys are widely used in aircraft and aerospace structures due to their high strength to density ratios. In such applications, the fracture toughness rather than the strength is often the factor which requires larger size sections and lower useful payloads. The response of the strength and toughness of titanium alloys has been analyzed generally without regard to the fracture mode or the effect of microstructure on the fracture mechanisms. Research on the fracture mechanisms in aluminum alloys[1] and steels[2] have shown that the toughness may be improved by decreasing the sizes of inclusions and sub-micron precipitates. The purpose of this investigation is to study the fracture mechanisms in titanium alloys which may lead to suggestions for the improvement of the fracture toughness without a corresponding loss in strength.

INTRODUCTION

Titanium alloys are generally characterized as α, β, or α + β alloys. The α-alloys consist of a structure of α grains. The α phase is the low temperature, hexagonal close-packed phase in unalloyed titanium and is stabilized in alloyed titanium by the α-stabilizing elements such as aluminum and oxygen. The β alloys consist mainly of a structure of β grains. The β phase is the high temperature, body-centered cubic phase in unalloyed titanium which becomes stable at lower temperatures with the addition of β-stabilizing elements such as molybdenum and zirconium. The β alloys are solution treated in or near the β phase field and quenched into the room temperature α + β field rapidly enough to prevent formation of large amounts of primary α. These alloys are strengthened by aging in the α + β field through formation of sub-micron size α precipitates. Thus, the classification of these alloys as β alloys is a misnomer. The α + β alloys are very similar to the β alloys except that the α + β alloys are usually solution treated in the α + β field which results in the formation of primary α. They are then aged to precipitate α in the β matrix.

A summary of the modes of fracture of various titanium alloys at room temperature is given by Williams, Boyer, and Blackburn.[3] Most of the alloys failed by dimpled rupture. This is the mode of fracture where

microscopic voids form at precipitates or impurity particles. These voids grow and finally coalesce, resulting in the final rupture. In titanium-aluminum α alloys, Williams, et al.[3] reported that alloys with less than 7 weight percent aluminum failed by dimpled rupture with a wide variation of dimple sizes attributed to the plastic anisotropy of the hexagonal close-packed matrix. No void nucleating particle could be identified. In the alloys in excess of 7 weight percent aluminum, there was a tendency for the fracture mode to be cleavage. The α + β alloy, Ti-8Al-1Mo-1V, was observed to fail by dimpled rupture but no void nucleating particle could be identified. A β alloy, Ti-11.6Mo, was shown to fail by dimpled rupture in both the solution treated and aged condition. Although the dimple size was smaller in the aged condition, no void nucleating particle was identified.

Since that publication, Greenfield and Margolin[4] systematically studied the fracture process of the α + β alloy, Ti-5.25Al-5.5V-0.9Cu-0.5Fe, in tensile samples. This alloy was heat treated to form various sizes of two different morphologies of primary α. The alloys failed by dimpled rupture and the voids were formed by interface separation of the primary α from the α + β matrix. As the size of the primary α particles increased, the voids initiated at lower strains and the void growth rate increased. Greenfield and Margolin[4] noted that while the primary α-matrix interface

acted as the void nucleation site, when voids approached another interface the void growth is stopped. Greenfield and Margolin stated that stress relief occurred when a void or crack approached an α particle. If this is the case, it would seem that voids would not grow from the α-matrix interface.

To date, the fracture mechanisms of the α and β alloys have not been systematically studied. The purpose of this investigation is to study the fracture process in the α alloy, Ti-5Al-2.5Sn, and the β alloy, Ti-11.5Mo-6Zr-4.5Sn, known as Beta III.

A. Ti-5Al-2.5Sn

This α alloy is based on the titanium-aluminum system. The currently accepted version of the titanium-aluminum phase diagram is that of Blackburn,[5] which is shown in Figure 1. This phase diagram was constructed from X-ray work and transmission electron microscopy. In addition to the α and β phases, there is an ordered α_2 phase. This is a phase based on Ti_3Al which has a DO_{19} hexagonal crystal structure. Quenching alloys with greater than 8 weight percent aluminum could not prevent the formation of α_2. Diffuse superlattice reflections were observed in thin foils with as low as 6 weight percent aluminum. This was interpreted as either short range order or α_2 precipitates smaller than 25 Å. Recently Namboodhiri, McMahon, and Herman[6] investigated this system

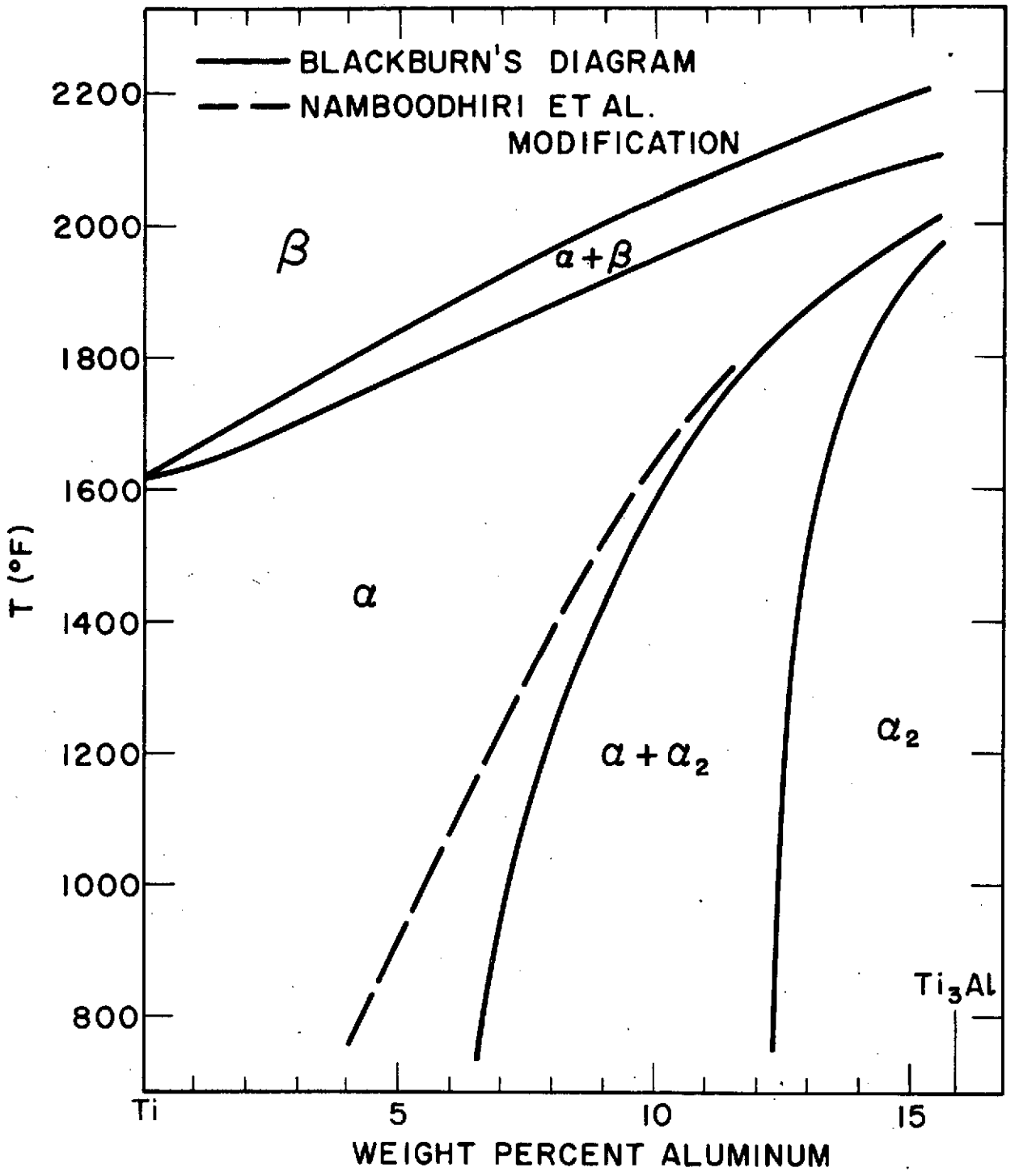

Figure 1 - Titanium Rich Portion of Ti-Al Phase Diagram

with electron microscopy and resistivity measurements. Their modification to Blackburn's phase diagram is also shown in Figure 1. The general shape of Blackburn's phase diagram was not altered but the $\alpha/\alpha+\alpha_2$ solvus was shifted to lower aluminum contents. Electrical resistivity measurements on a 4 weight percent aluminum alloy were made after room temperature deformation. The resistivity passed through a minimum value with increasing deformation and was interpreted as the presence of short range order. The difference between these two phase diagrams is a matter of current controversy. No substantial work has been done on the titanium-aluminum-tin phase diagram, but the titanium-tin phase diagram is similar to the titanium-aluminum diagram in that an ordered phase Ti_3Sn which has a DO_{19} crystal structure has been observed.[27]

Deformation studies on Ti-Al alloys have been carried out by Truax and McMahon,[7] and Blackburn and Williams.[8] Both studies showed that as the aluminum content was increased so were the flow stresses of the materials. Blackburn's material with a higher oxygen content than Truax and McMahon's alloys had higher flow stresses and at similar aluminum levels exhibited more planar slip. These results are supported by the work of Conrad, Okasaki, Gadgil, and Jon[9] on the Ti-O system. In alloys up to 8 weight percent aluminum, the mode of fracture was dimpled rupture.[7] Neither investigation observed the alloys to twin. In the Blackburn and Williams study,[8] a 6 weight percent aluminum alloy

was observed to deform by the motion of pairs of dislocations, but no α_2 precipitation was observed. The rapid strengthening with aluminum content in alloys with less than 6 weight percent aluminum was interpreted as evidence of short range order.

The alloy Ti-5Al-2.5Sn is generally used for cryogenic applications. While its room temperature yield stress is only about 100 ksi, its liquid hydrogen (-423°F) yield stress is approximately twice that level. The addition of aluminum and tin reduced the density of Ti-5Al-2.5Sn (0.161 lb/in^3) to less than that of unalloyed titanium (0.163 lb/in^3). Shannon and Brown[10] characterized the strength and crack tolerance of this alloy over the temperature range from room temperature to that of liquid hydrogen. They also investigated the effect of interstitial levels and cooling rate from a 1500°F mill anneal. The extra-low interstitial grades have yield and tensile strengths less than the commercial, higher interstitial material. The crack tolerance as reflected in the notched tensile strength dropped suddenly at about -150°F for the commercial material, while the notched strength of the extra low interstitial (ELI) material did not decrease suddenly until about -320°F. At -423°F, furnace cooled ELI material possessed lower crack tolerance than the air-cooled ELI alloy which was attributed to the presence of ordering. Erbin[11] noted that increasing the iron content of ELI Ti-5Al-2.5Sn

above 0.2 weight percent drastically decreases the notched tensile strength to yield strength ratio over the cryogenic temperature range studied by Shannon and Brown. Christian, Hurlich, Chafey, and Watson[12] observed an increase in the amount of a second phase in Ti-5Al-2.5Sn as the iron level increased. Interstitial levels of 0.07 to 0.50 weight percent seemed to have no affect on this second phase. Christian, et al.[12] noted that low-oxygen, low-iron material possessed better notched properties at -423°F than either medium oxygen, medium iron, or low oxygen, high iron material. Curtis, Boyer, and Williams[13] identified a second phase in Ti-5Al-2.5Sn as iron-stabilized β.

B. Beta III (Ti-11.5Mo-6Zr-4.5Sn)

This alloy is basically a Ti-Mo alloy. That system has the complication of forming the ω phase upon quenching from the β phase field. Williams, Hickman, and Marcus[14] have shown that an 11.5 weight percent molybdenum alloy aged at low temperatures failed in a brittle fashion before the macroscopic yield stress was reached. The addition of zirconium and tin do not effect the kinetics of the formation of the hexagonal ω phase but do limit the amount which can be formed.[15] Froes, Capenos, and Wells[16] have constructed the Ti-Mo section of the Beta III phase diagram which is shown in Figure 2. The alloys used in their alloy partition study had an oxygen content about twice that of the commercial alloy, so the β transus (α + β/β solvus line) may be higher

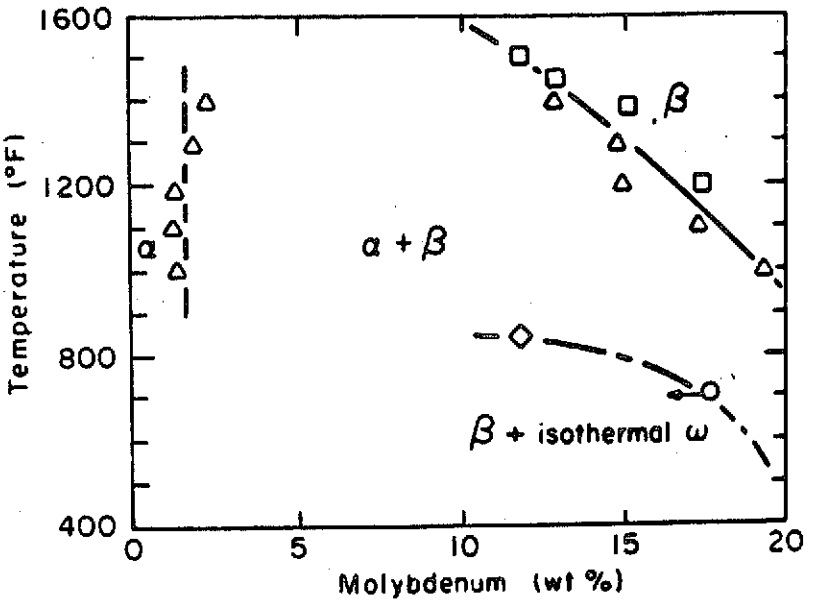

Ti-Mo section of the Beta III phase diagram.

△ Partition data.
○ Behavior of 17.3% Mo - Beta III on 700F aging.
◇ Upper limit of isothermal omega in regular Beta III.
□ Beta transus for 0.280_2 - Beta III type alloys.

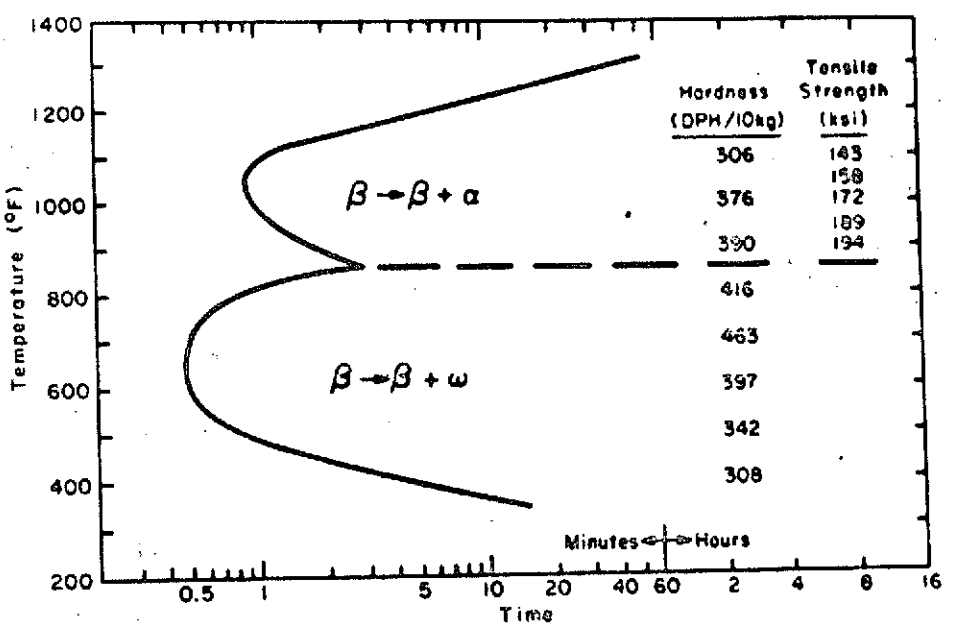

Time-Temperature-Transformation Characteristics of Beta III

Figure 2 βIII Phase Diagram[16] and Transformation Kinetics[17]

than usual as a result of the α-stabilizing element oxygen. Also shown in Figure 2 are the transformation kinetics and maximum hardness and tensile strengths of Beta III.[17] This alloy approaches the strength of low alloy steels, while it has considerably lower density (0.183 vs. 0.283 lb/in^3). When aged to these strength levels, this alloy is intended for ambient temperature structural applications. Above 850°F, the β' phase will transform to a β + α microstructure; while below that temperature, the embrittling ω phase will form.

Feeney and Blackburn[18] characterized the effect of microstructure on the strength and toughness of Beta III. The material was solution treated above the β transus and aged in both the β + α and β + ω phase fields. Transmission electron microscopy revealed the as quenched material had a structure of ω precipitates smaller than 25 Å in beta grains with sizes ranging from 0.22 to 0.30 mm. Material aged at 900°F passed through a strength maximum of about 160 ksi between 2 and 20 hours. At this strength level, the material had a fracture toughness of about 40 ksi√in. The α-aged alloys failed by dimpled rupture but no void nucleating particle was observed or identified. The 700°F ω-aged material failed in a brittle fashion short of macroscopic yielding in tension samples aged for 2 hours or more. Even though the fracture was macroscopically brittle, the fracture mode was dimpled rupture. No void nucleating particle was

was observed. The K_{Ic} values for the $\beta + \omega$ microstructure decreased with increasing aging times at 700°F. Guernsey, Petersen, and Froes[19] have reported that the results of Feeney and Blackburn[18] do not fully reflect the properties of Beta III. The strength and toughness of the α-aged alloy can be increased to 180 ksi and 60 ksi$\sqrt{in.}$, respectively, by heavy deformation prior to a sub-β transus solution treatment. This will result in an unrecrystallized β microstructure with only minor amounts of primary α along β grain boundaries. Upon aging, the α will precipitate on the remaining dislocations which will cause finer precipitates resulting in improved strength and toughness.

C. Scope of this investigation

The purpose of the current investigation is to study the effect of microstructure on the fracture mode and fracture toughness of the α alloy, Ti-5Al-2.5Sn, and Beta III. The α alloy will be investigated with particular reference to cryogenic applications so the fracture mechanism will be studied at room temperature, -320°F, and -423°F. Ti-5Al-2.5Sn will be investigated in both commercial and extra low interstitial grades with parts of each plate having been either air cooled or furnace cooled, similar to the work of Shannon and Brown.[10] Beta III will be investigated in a sub-β transus solution treated condition followed by either α or ω aging. The comparison between $\beta + \alpha$ and $\beta + \omega$

microstructures at the same yield strength level will be made at room temperature.

The mechanical properties of both alloys will be measured using smooth tension and plane strain fracture toughness tests. The microstructures will be characterized using light and electron metallography along with microprobe or X-ray techniques when appropriate. The fracture mode will be determined using electron microscope replicas. The fracture mechanism will be investigated by studying metallographic sections of both smooth and notched samples using techniques similar to the ones utilized in the investigation of the fracture processes in aluminum alloys[1] and steels[2] in this laboratory.

What follows is a progress report on the investigation to date.

MATERIALS

The Ti-5Al-2.5Sn alloys were obtained from NASA Lewis Research Center in the form of one inch thick rolled plate. Both commercial and extra low interstitial (ELI) grades were received with sections of each plate having been either air cooled or furnace cooled from a 1500°F mill anneal. The chemical specifications, heat analyses, and two check analyses on each plate are shown in Table I. The oxygen level in the ELI material is about one-third that of commercial grade and the ELI iron content is about one half of the commercial iron level. The microstructures of these alloys as revealed in the optical microscope is shown in Figure 3. A second phase was revealed by etching in an $HF-HNO_3-H_2O$ solution of the ratio of 1:2:100. In the micrographs, the rolling direction is in the vertical direction and the transverse direction is horizontal. The effect of cooling rate cannot be observed in the microstructure at this magnification. The ELI material has a much lower volume fraction of the second phase than the commercial Ti-5Al-2.5Sn alloys. The size of the particles in the ELI plates is about 2 microns while the particle diameters in the commercial material is about 5 microns. The ELI material also has a larger α grain size. From the iron content of these alloys and the work of Curtis, Boyer, and Williams,[13] it is believed this phase is iron-stabilized beta.

TABLE I

CHEMICAL ANALYSES OF Ti - 5 Al - 2.5 Sn ALLOYS
(Weight Percent)

	Al	Sn	Fe	Mn	O	C	N	H
Commercial Specification	4.0/6.0	2.0/3.0	0.50 Max	0.30 Max	0.20 Max	0.15 Max	0.07 Max	0.003/0.020
Commercial Heat Analysis	5.1	2.5	0.28	0.006	0.16	0.024	0.023	0.009
Commercial, AC* Check Analysis	5.22	2.47	0.300	0.002	0.164	0.0140	0.0163	0.0072
Commercial, FC† Check Analysis	5.24	2.47	0.270	0.002	0.169	0.0120	0.0172	0.0042
ELI Specification	4.7/5.6	2.0/3.0	0.1/0.2	--	0.12 Max	0.08 Max	0.05 Max	0.0125 Max
ELI Heat Analysis	5.0	2.6	0.16	0.006	0.086	0.023	0.010	0.006
ELI, AC * Check Analysis	5.09	2.44	0.140	0.002	0.054	0.0057	0.0098	0.0056
ELI, FC † Check Analysis	5.10	2.47	0.145	0.002	0.052	0.0041	0.0098	0.0050
Maximum Error in Check Analysis	0.200	0.150	0.010	0.0005	0.010	0.0010	0.0010	0.0010

* Air Cooled
† Furnace Cooled

Commercial, Air Cooled

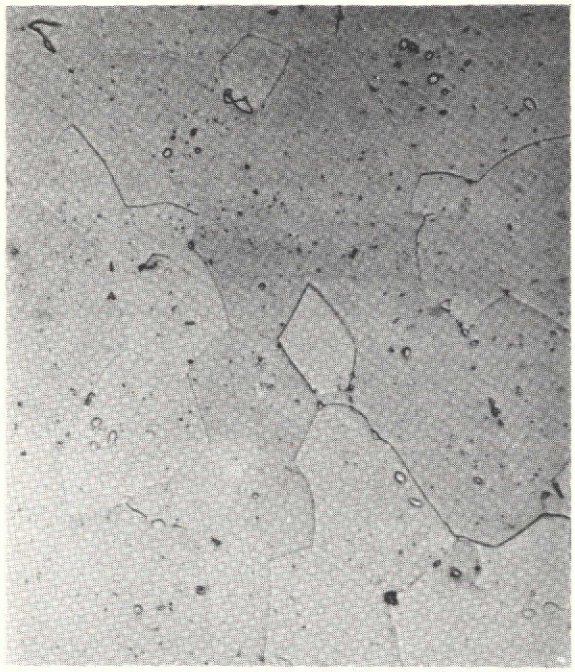

Commercial, Furnace Cooled

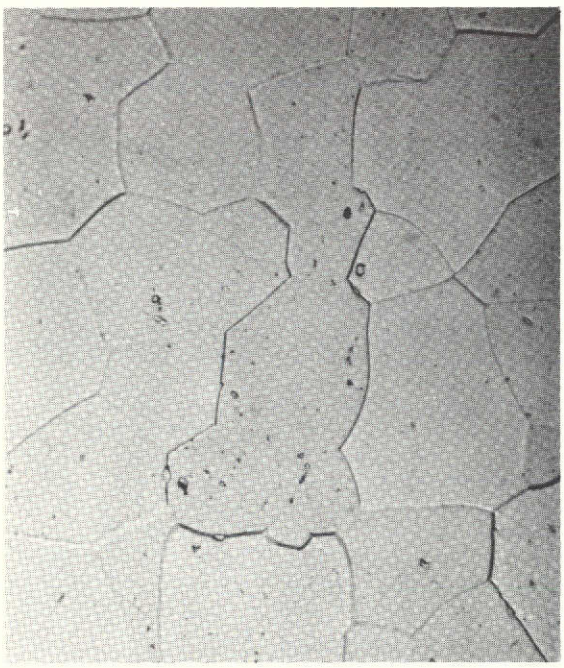

ELI, Air Cooled

ELI, Furnace Cooled

20μ

Figure 3: Micrographs of the Ti-5Al-2.5Sn Alloys. The rolling direction is vertical and the transverse direction is horizontal.

This page is reproduced at the back of the report by a different reproduction method to provide better detail.

The Beta III (Ti-11.5Mo-6Zr-4.5Sn) material was procured from Colt Industries in the form of 0.8 inch thick plate. The chemical specification, heat analysis, and check analysis are shown in Table II. This plate was fabricated from ingot form to a 4-1/2 inch thick slab by forging, starting at 2000°F. Following conditioning, the slab was hot rolled to 0.8 inches thick starting at 2050°F but finishing at a low temperature to produce a worked structure. The plate was then given a sub-β transus solution treatment at 1325°F for 15 minutes followed by a water quench. The microstructure of the solution treated microstructure is shown in Figure 4. This is a light micrograph of the structure etched with a 30% HNO_3, 2% HF, H_2O solution with the longitudinal orientation in the horizontal direction and the transverse direction displayed vertically. The darkly etched areas are regions of non-recrystallized β, while the lighter areas are recrystallized. Small amounts of primary α can be seen along a few of the recrystallized β grain boundaries. An energy dispersion detector on a scanning electron microscope was used to analyze the light and dark etched regions. No differences in molybdenum, zirconium, or tin could be observed. Microhardness tests were performed on the two regions and revealed that the 3 kilogram Vickers hardness of the dark grains was 307 while that of the light region was 295. This corresponded to an indentation diameter of about 130 microns. Statistical analysis revealed that the

TABLE II

CHEMICAL ANALYSES OF BETA III (Ti - 11.5 Mo - 6 Zr - 4.5 Sn)
(Weight Percent)

	Mo	Zr	Sn	Fe	O	H	C	N
Specification	10.00/13.00	4.50/7.50	3.75/5.25	0.35 Max	0.18 Max	0.020 Max	0.100 Max	0.050 Max
Heat Analysis	10.2	5.8	4.7	0.03	0.13	0.0143	0.02	0.014
Check Analysis	10.82	5.56	4.60	0.050	0.130	0.0027	0.0104	0.0110
Maximum Error in Check Analysis	0.200	0.100	0.150	0.010	0.0100	0.0010	0.0010	0.0010

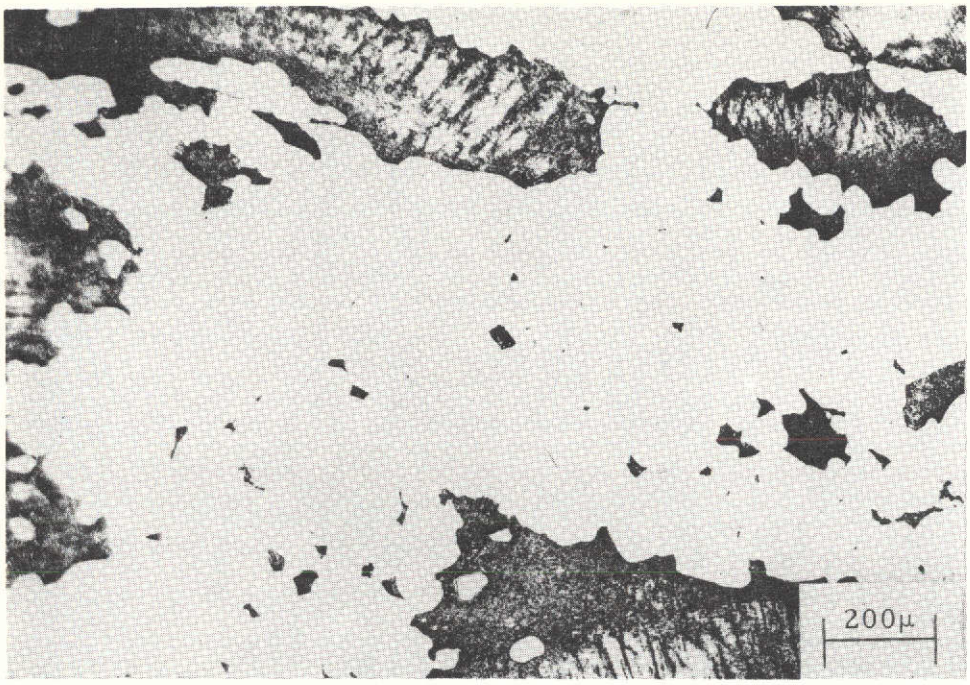

Figure 4: Solution Treated Beta III Structure. The longitudinal direction is horizontal.

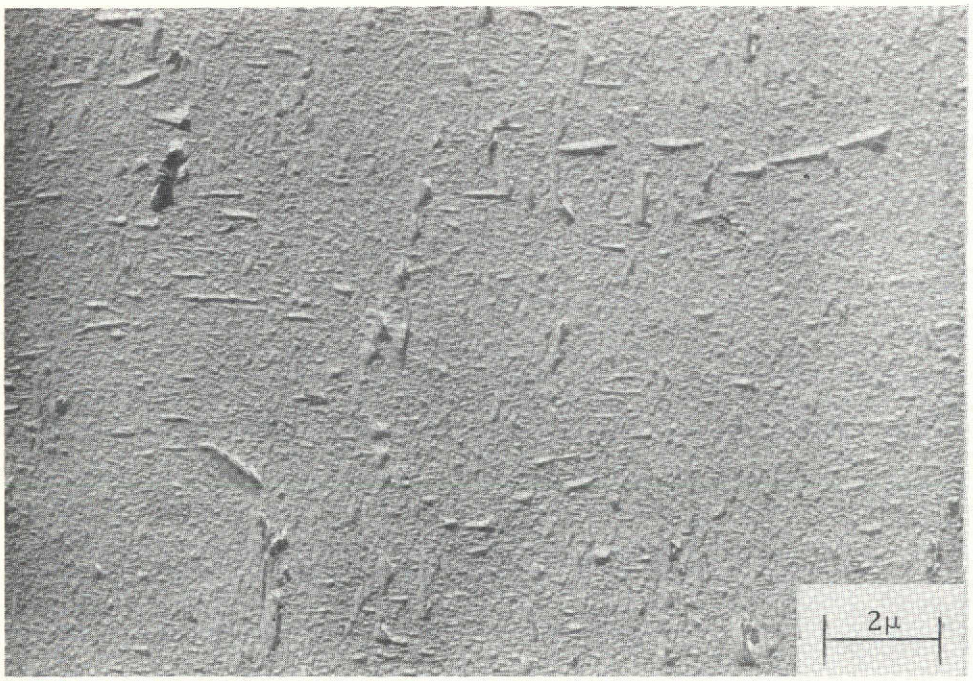

Figure 5: The α-Aged Structure of Beta III.

This page is reproduced at the back of the report by a different reproduction method to provide better detail.

probability that the hardnesses are different is in excess of 99%. As one would expect, the unrecrystallized grains were slightly harder than the recrystallized ones.

As suggested by Froes,[20] the Beta III was α-aged using a 925°F 8-hour aging treatment with a slow heating rate. Froes reports that this treatment results in a better strength/ductility combination than the previously recommended 950°F 8-hour aging treatment. Work is currently underway to age Beta III at 700°F to form a β + ω microstructure at the same yield strength level as the α-aged material. The times used to characterize this aging process were 0.5, 1.0, 1.67, 3.0, 5.5, and 10.0 hours.

The microstructure of the 925°F α-aged Beta III is shown in Figure 5, as revealed in an electron microscope replica from a metallographic sample etched in a 2% HF solution. Primary α about one micron long can be observed along with the much finer α precipitate in the background which forms during the aging treatment.

MECHANICAL TESTING

The mechanical properties of these alloys are to be characterized using tension tests and plane strain fracture toughness tests. Tests are to be performed at room temperature (70°F), liquid nitrogen temperature (-320°F), and liquid hydrogen temperature (-423°F). The liquid hydrogen tests are to be performed at a NASA Lewis Research Center facility and the other tests will be performed in this laboratory. Both facilities meet the requirements of the ASTM standard for fracture toughness testing.[21] Because of frequent problems with resistance strain gages at cryogenic temperatures, the K_{Ic} specimen clip gage and extensometer for tension tests at all temperatures will use linear variable differential transformers (LVDT). The LVDT used in this laboratory has a linear range of plus or minus 0.100 inch so that by properly setting the null point and using full-scale zero suppression electronics, the LVDT will have a linear range of 0.200 inch.

The method used to calibrate the LVDT is that developed by Shannon and co-workers.[22] At two different temperatures (for example, 70°F and -320°F), a plot of output versus phase was generated at constant displacement and constant gain such as the schematic shown in Figure 6a. The crossover point, as noted as Point A in Figure 6a, is the phase setting for that particular gain where the calibration is the same at both

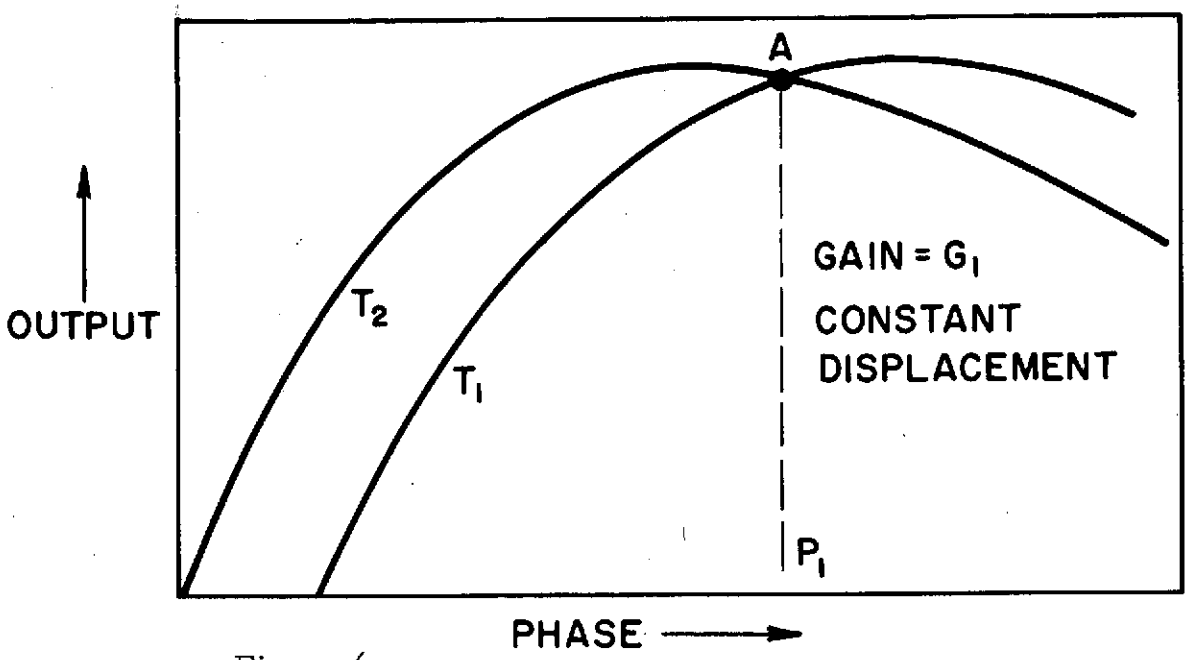

Figure 6a

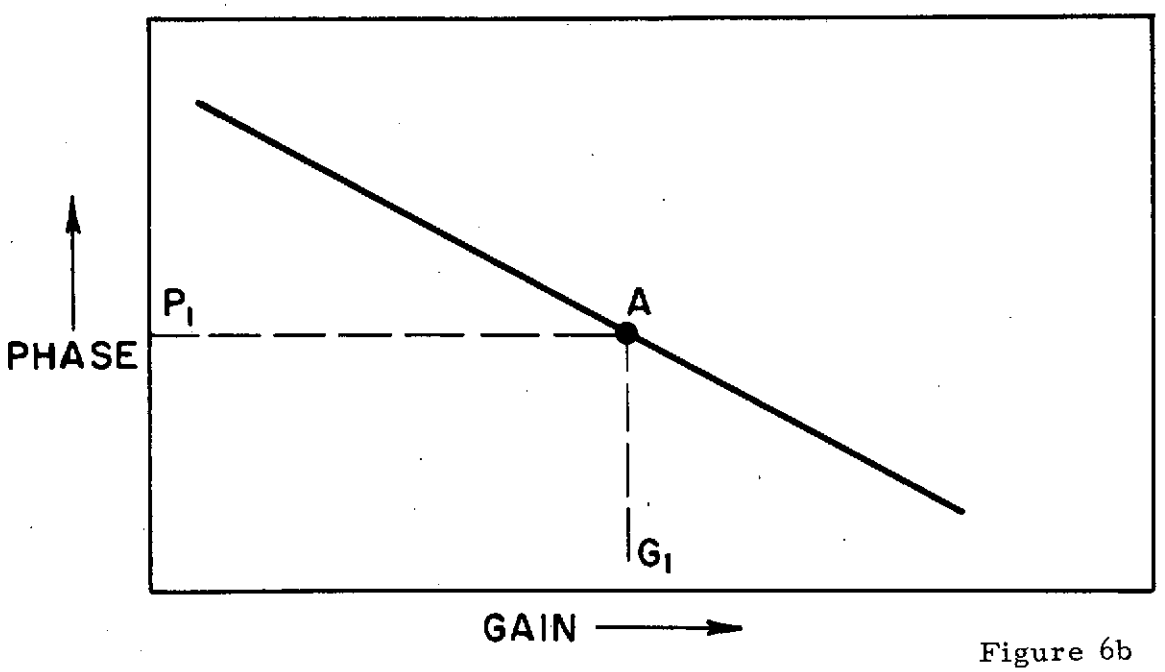

Figure 6b

Figure 6 Schematic Showing Technique for Calibration of LVDT at Two Temperatures

temperatures. This procedure is repeated at several gain values so that a plot of phase versus gain can be constructed where the calibration at both temperatures is the same. A schematic of such a plot is shown in Figure 6b. The magnification for a given test is picked by the proper gain and chart sensitivity setting. A figure like the one in Figure 6b will be used to determine the appropriate phase setting. The LVDT can then be calibrated at room temperature for cryogenic applications.

The yield stress, ultimate tensile strength, fracture stress, uniform strain, and fracture strain were measured using round tensile samples. Tension tests were conducted by monitoring the load and extension by means of a fast response load cell and an LVDT extensometer. After necking began, the extensometer was removed and the load was monitored as function of time. The samples were strained slightly beyond the previous strain increment and unloaded. The load prior to unloading was noted and the minimum specimen diameter in the necked region was measured with a point micrometer. This process was repeated several times before fracture occurred. Using these data, a true stress-true plastic strain curve could be plotted using standard calculations.[23]

As noted by Bridgman,[24] there is a region of hydrostatic tension in the neck of a tensile sample. If a flow curve is to represent the flow

characteristics of the material being tested, this hydrostatic component must be subtracted from the measured axial stress. Bridgman[24] developed the following expression for the correction factor (F) by which the measured true stress in a tension sample must be multiplied to calculate the Bridgman corrected true stress:

$$F = 1/\{ [1 + 2 (R/a)] \log [1 + 1/2 (a/R)] \} \qquad \text{Eq. (1)}$$

where a = Minimum radius of the speciman in the necked region

R = Radius of curvature of the neck

Thus, the correction factor is a function only of the neck geometry. Bridgman showed that the plot of a/R against strain was linear up to strains of unity for a wide variety of steels.

There is no reason to expect that Bridgman's correlation for steels should be applicable to the titanium alloys being studied here, so a plot of a/R against strain was constructed for several Ti-5Al-2.5Sn alloys tested at room temperature. The a/R value was determined by placing a necked specimen on a shadowgraph with a magnification of 20 times and tracing the observed neck on a piece of tracing paper. The radius of curvature was measured from a geometric construction at the neck. From this datum, the a/R value was calculated. Figure 7 shows a plot of a/R for the room temperature tests on the air-cooled Ti-5Al-2.5Sn alloys and Bridgman's data on steels. Also shown in the figure is the line

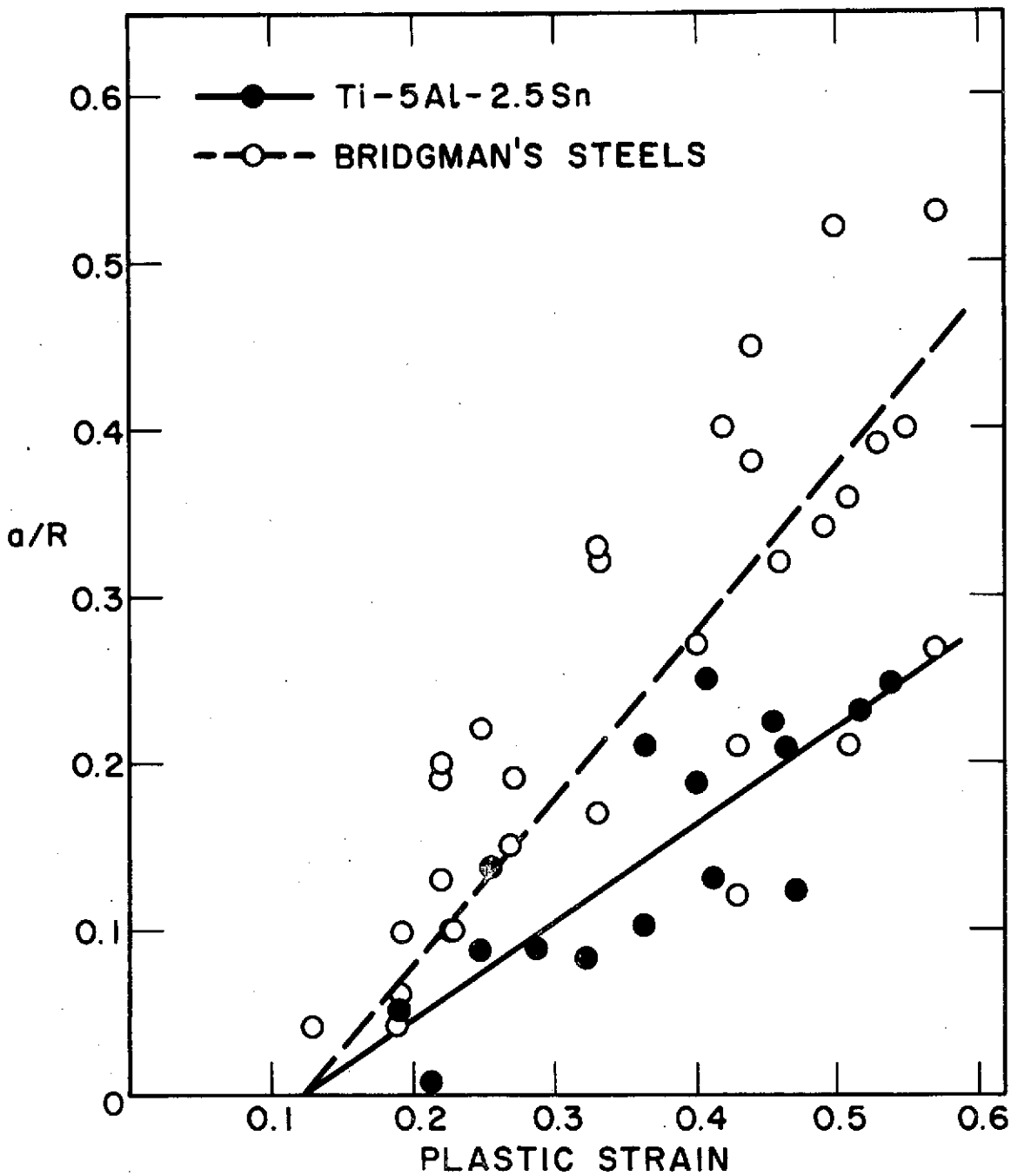

Figure 7 a/R as a Function of Strain for Ti-5Al-2.5Sn and Steels[24]

constructed by Bridgman and a linear least square regression line for the titanium data. Although the scatter for both materials is quite wide, it is apparent that the a/R ratios for titanium alloys are less than those of steels at the same strain. The regression equation for the titanium alloys is given below:

$$a/R = -0.072 + 0.589\,\epsilon \qquad \text{Eq. (2)}$$

where ϵ = true plastic strain.

This expression was used to calculate a/R; and when the calculated value of a/R was positive, the Bridgman correction factor was calculated from Eq. (1).

Figure 8 shows the engineering stress, true stress, and Bridgman corrected true stress plotted against the true plastic strain for room temperature tests on the furnace cooled ELI Ti-5Al-2.5Sn alloy. The Bridgman corrected stress (σ) was fitted to an equation of the form:

$$\sigma = \sigma_o + A\epsilon^m \qquad \text{Eq. (3)}$$

where σ_o, A, and m were evaluated by regression analysis. An equation of this form has been used for the flow curves of Ti-Al[7] and Ti-O[9] alloys. The stresses calculated from the regression analysis were usually within 2 percent of the experimental values.

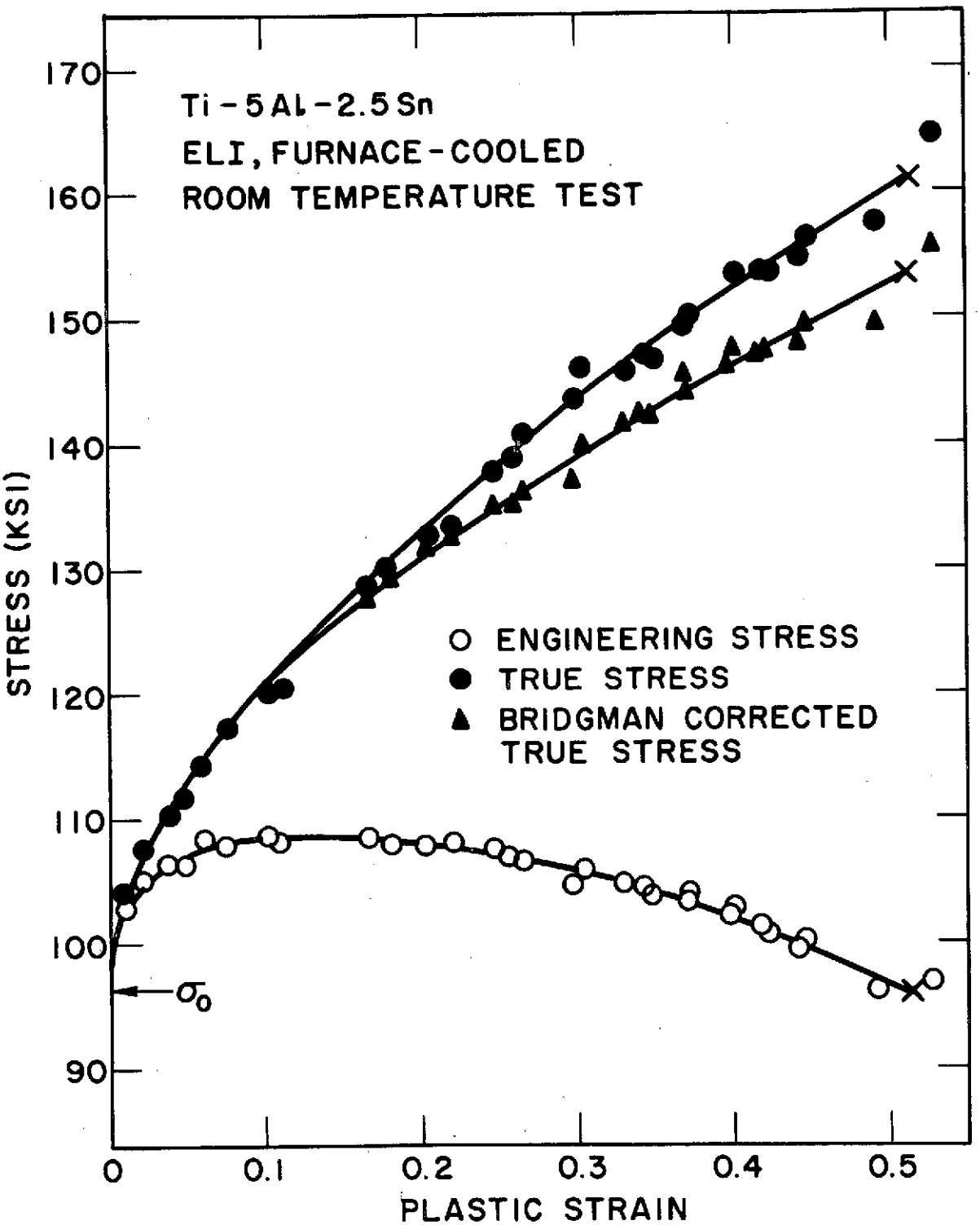
Ti-5Al-2.5Sn
ELI, FURNACE-COOLED
ROOM TEMPERATURE TEST
ENGINEERING STRESS
TRUE STRESS
BRIDGMAN CORRECTED TRUE STRESS
σ_o
STRESS (KSI)
PLASTIC STRAIN
170
160
150
140
130
120
110
100
90
0
0.1
0.2
0.3
0.4
0.5

Figure 8

The plane strain fracture toughness tests are to be conducted in accordance to ASTM standard E399-72.[21] The LVDT clip gauge will be attached to the specimen on detachable knife edges.

The tensile tests on these alloys will be performed on longitudinal samples. The K_{Ic} specimens will have the major stress axis oriented along the longitudinal direction and the crack will propagate in the transverse direction.

The tension specimens at 70°F and -320°F will be 0.252 inch diameter samples, while those tested at -423°F will be 0.505 inch diameter samples. The tension tests at liquid hydrogen temperatures will not be interrupted for flow curves determinations. The fracture toughness tests at 70°F and -320°F will use compact tension samples, but the -423°F tests will use 3-point bend specimens. The Ti-5Al-2.5Sn K_{Ic} samples will be 1 inch thick and the Beta III specimens will be 0.75 inch thick. These thicknesses should be sufficient to meet the ASTM thickness criteria in all cases with the possible exception of the 70°F Ti-5Al-2.5Sn tests.

The mechanical testing of these alloys has not been completed but the results to date are shown in Tables III and IV. No fracture toughness tests have been completed and no liquid hydrogen test results have

TABLE III

MECHANICAL TEST RESULTS: STRENGTHS AND DUCTILITIES

Alloy	Test Temperature (°F)	Yield Stress (ksi)	Tensile Strength (ksi)	Fracture Strength (ksi)	Fracture Strain	Uniform Strain
Ti-5Al-2.5Sn Commercial Air Cooled	70	126.9 ± 0.5	133.8 ± 0.3	178.5 ± 0.6	0.434 ± 0.040	0.086 ± 0.004
	- 320	194.5	207.8	262.9	0.304	0.080
Ti-5Al-2.5Sn Commercial Furnace Cooled	70	127.9 ± 0.8	132.6 ± 0.3	166.1 ± 5.9	0.328 ± 0.055	0.091 ± 0.001
Ti-5Al-2.5Sn ELI Air Cooled	70	102.1 ± 0.8	110.2 ± 1.1	154.8 ± 0.3	0.528 ± 0.011	0.076 ± 0.033
	- 320	171.4	181.5	233.9	0.338	0.103
Ti-5Al-2.5Sn ELI Furnace Cooled	70	98.9 ± 0.7	108.4 ± 0.4	152.5 ± 4.2	0.512 ± 0.025	0.107 ± 0.003
Beta III α-Aged	70	185.7 ± 1.8	196.6 ± 0.6	214.7 ± 2.2	0.109 ± 0.009	0.029 ± 0.002

TABLE IV

MECHANICAL TEST RESULTS
FLOW CURVE LEAST SQUARE REGRESSION TO THE FORM

$$\sigma = \sigma_o + A\varepsilon^m$$

Alloy	Test Temperature	σ_o (ksi)	A (ksi)	m
Ti-5Al-2.5Sn Commercial Air-Cooled	70°F	120.5 ± 0.4	82.9 ± 1.4	0.47
Ti-5Al-2.5Sn Commercial Furnace Cooled	70°F	123.4 ± 0.3	81.2 ± 1.3	0.55
Ti-5Al-2.5Sn ELI Air Cooled	70°F	98.0 ± 0.4	77.5 ± 1.4	0.50
Ti-5Al-2.5Sn ELI Furnace Cooled	70°F	96.4 ± 0.2	81.5 ± 0.4	0.54
Beta III α-Aged	70°F	150.6 ± 1.8	96.3 ± 3.8	0.17

been reported. The tables show standard deviations in all cases where multiple tests have been completed.

The strength and tensile ductility levels of these alloys are shown in Table III. The yield and tensile strengths of the Ti-5Al-2.5Sn alloys are almost identical to the results of Shannon and Brown.[10] As expected, the strength of the commercial alloys is greater than the ELI material. Also shown is the improvement of strength and loss of ductility with decreasing test temperature. The strength and ductility for the α-aged Beta III are typical for this heat treatment.

The constants resulting from the flow curve regression analysis are shown in Table IV. The data for the Ti-5Al-2.5Sn alloys suggest that the effect of increasing the interstitial level is to raise the apparent elastic limit (σ_o) without greatly effecting A and m which control the rate of strain hardening. The value of m is close to 0.5 which agrees with the results of Conrad, et al.[9] on Ti-O alloys and the work of Truax and McMahon[7] on low aluminum Ti-Al alloys. These results suggest that the higher strength of the commercial Ti-5Al-2.5Sn alloys is primarily a result of the increased interstitial level and not the iron stabilized β resulting from higher iron content.

The Ti-5Al-2.5Sn alloys room temperature flow curves are shown in Figure 9. These flow curves are a result of the regression analysis and

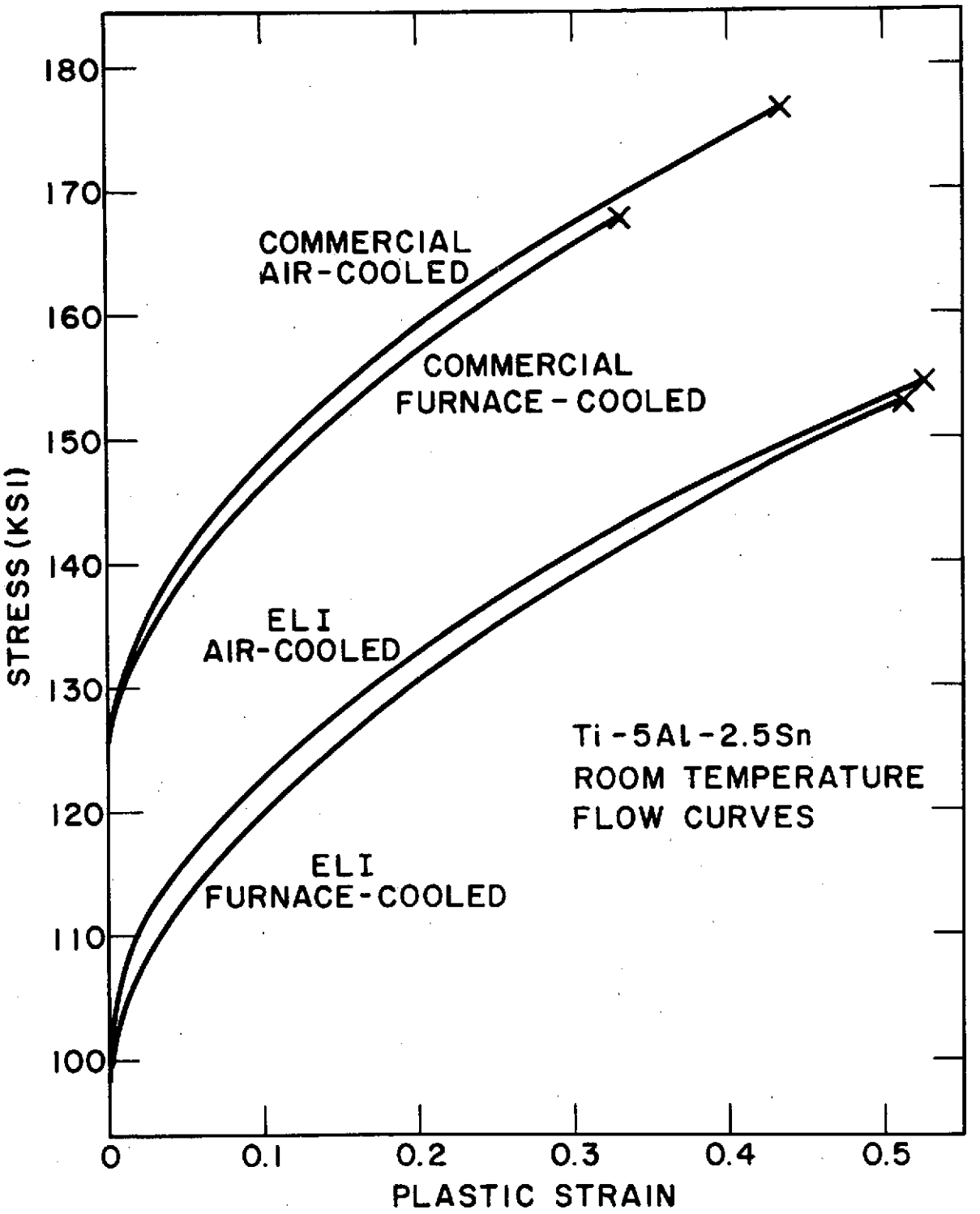
180
170
160
150
140
130
120
110
100
STRESS (KSI)
COMMERCIAL
AIR-COOLED
COMMERCIAL
FURNACE-COOLED
ELI
AIR-COOLED
ELI
FURNACE-COOLED
Ti-5Al-2.5Sn
ROOM TEMPERATURE
FLOW CURVES
0
0.1
0.2
0.3
0.4
0.5
PLASTIC STRAIN

Figure 9

are terminated at the average fracture strain. It is apparent furnace cooling and/or increased interstitial level results in reduced tensile ductility. The strengthening effect of the interstitials can be seen as simply raising the flow curve. Other than the extent of the curve, the rate of cooling from the annealing temperature has virtually no effect on the room temperature flow curves of Ti-5Al-2.5Sn alloys.

The engineering and true stress values are shown as a function of true plastic strain for the α-aged Beta III alloy in Figure 10. No neck was observable with the naked eye so no Bridgman correction was made. The fracture strain of this alloy is below the value which would result in a positive a/R according to Equation 2. Note in Table IV that the value of m is much different than the 0.5 value normally observed in the α alloys.

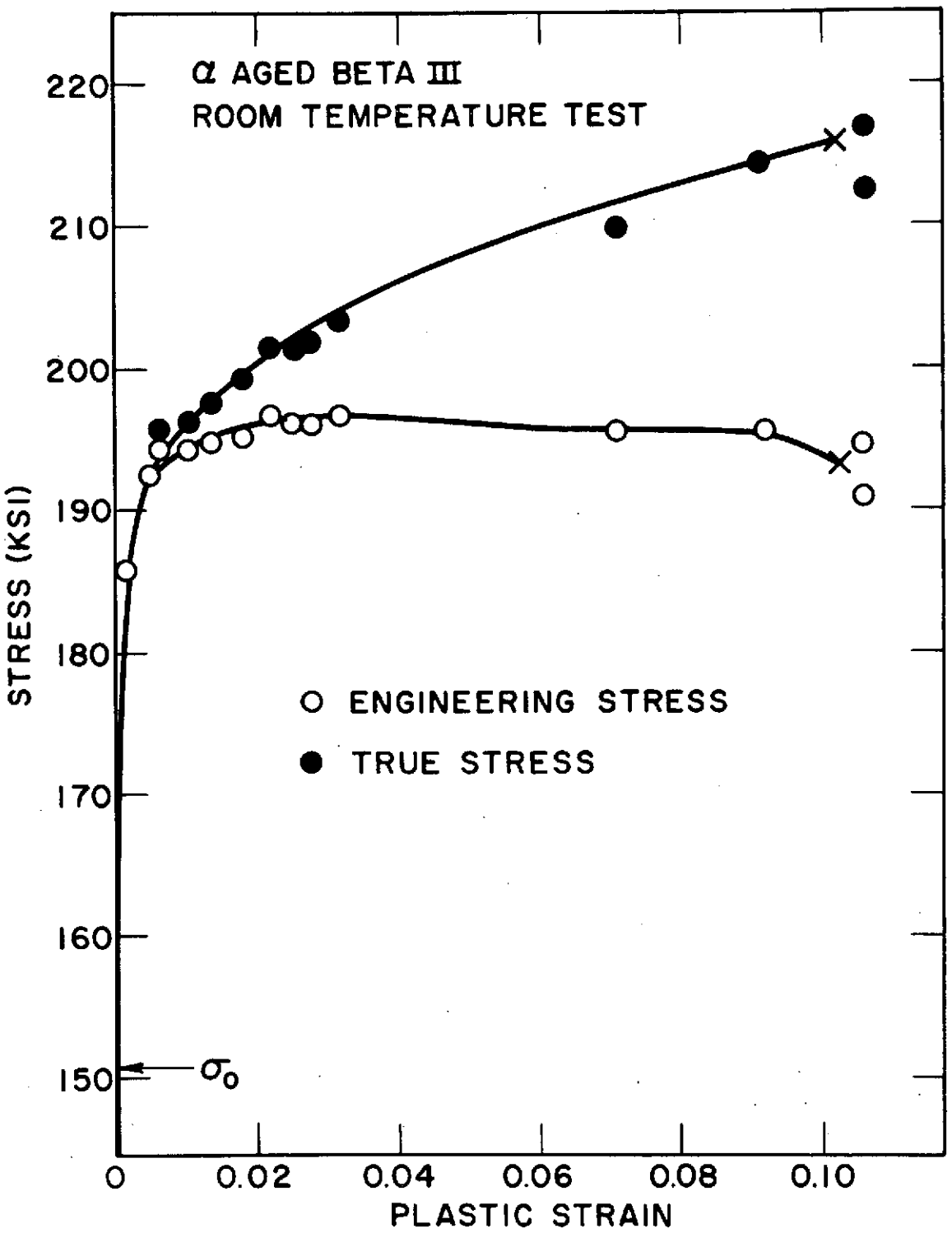
α AGED BETA III
ROOM TEMPERATURE TEST
220
210
200
190
180
170
160
150
STRESS (KSI)
ENGINEERING STRESS
TRUE STRESS
σo
0
0.02
0.04
0.06
0.08
0.10
PLASTIC STRAIN

Figure 10

FRACTOGRAPHY

The fracture surfaces of these alloys are to be studied using two-stage, platinum-carbon electron microscope replicas. To date, emphasis has been placed on the air-cooled Ti-5Al-2.5Sn alloys. All the fractographs shown here were taken from tensile fracture surfaces.

Typical fractographs of the room temperature and liquid nitrogen tensile fracture surfaces of the commercial Ti-5Al-2.5Sn alloy are shown in Figures 11 and 12. Both alloys failed by dimpled rupture but the -320°F fracture surface had more step-like features which could be observed when the fractographs were viewed in stereo pairs. These indicate the possible participation of planar slip or twinning in the fracture process. The room temperature fracture surface of this alloy often had large regions covered with marks known as serpentine glide, such as the region shown in Figure 13. This feature is a result of slip near the free surface of a void wall so that the slip traces appear on the fracture surface. Figure 14 shows a particle in the bottom of a dimple which participated in the initiation of a void on the room temperature fracture surface. It does not appear that the particle cracked so it is likely that this void was initiated by the interface separation. There was not a particle in every void. Similar features were also identified on the -320°F fracture surface. The particle shown in Figure 14 has a size on the order of the second

Figure 11: Fractograph of the Commercial, Air-Cooled Ti-5Al-2.5Sn Alloy from a Room Temperature Tensile Test

Figure 12 Fractograph of a Commercial, Air-Cooled Ti-5Al-2.5Sn Alloy from a Liquid Nitrogen Temperature Tensile Test

This page is reproduced at the back of the report by a different reproduction method to provide better detail.

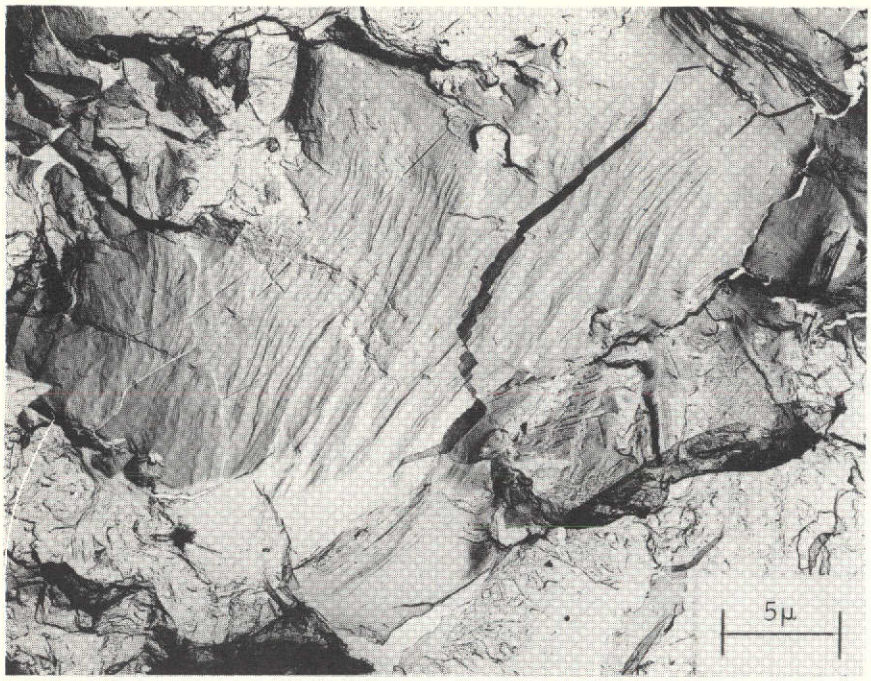

Figure 13 Serpentine Glide in a Dimple on the Room Temperature Tensile Fracture of Commercial, Air-Cooled Ti-5Al-2.5Sn Alloy.

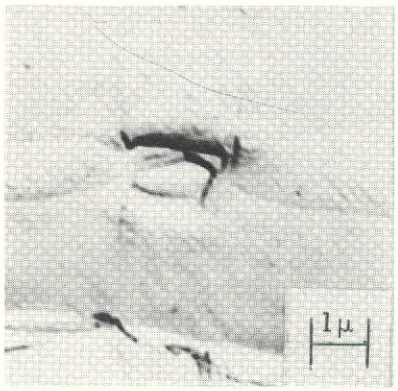

Figure 14 A Particle in a Dimple on the Room Temperature Fracture Surface of a Commercial, Air-Cooled Ti-5Al-2.5Sn Alloy.

This page is reproduced at the back of the report by a different reproduction method to provide better detail.

phase observed in this alloy. The iron stabilized β phase may act as the nucleation site for voids in the tensile fracture process. This point is better resolved by metallographic sectioning of fracture tensile specimens later in this report.

The room temperature and -320°F fractographs for the air-cooled ELI Ti-5Al-2.5Sn alloy are shown in Figures 15 and 16. In both cases, the tensile samples failed by dimpled rupture. The greater ductility is reflected in the greater dimple depth of the room temperature fracture surface. No step-like features similar to the ones observed in the -320°F commercial alloy were observed. Outlines of the second phase particles were also observed in the dimples on fracture surfaces of this alloy.

A typical fractograph of the α-aged Beta III is shown in Figure 17. Although this alloy failed with no appreciable necking, the mode of fracture is dimpled rupture. No void nucleating particle could be observed on the fracture surface.

Figure 15: Fractograph of the ELI Air-Cooled Ti-5Al-2.5Sn Alloy from a Room Temperature Tensile Test.

This page is reproduced at the back of the report by a different reproduction method to provide better detail.

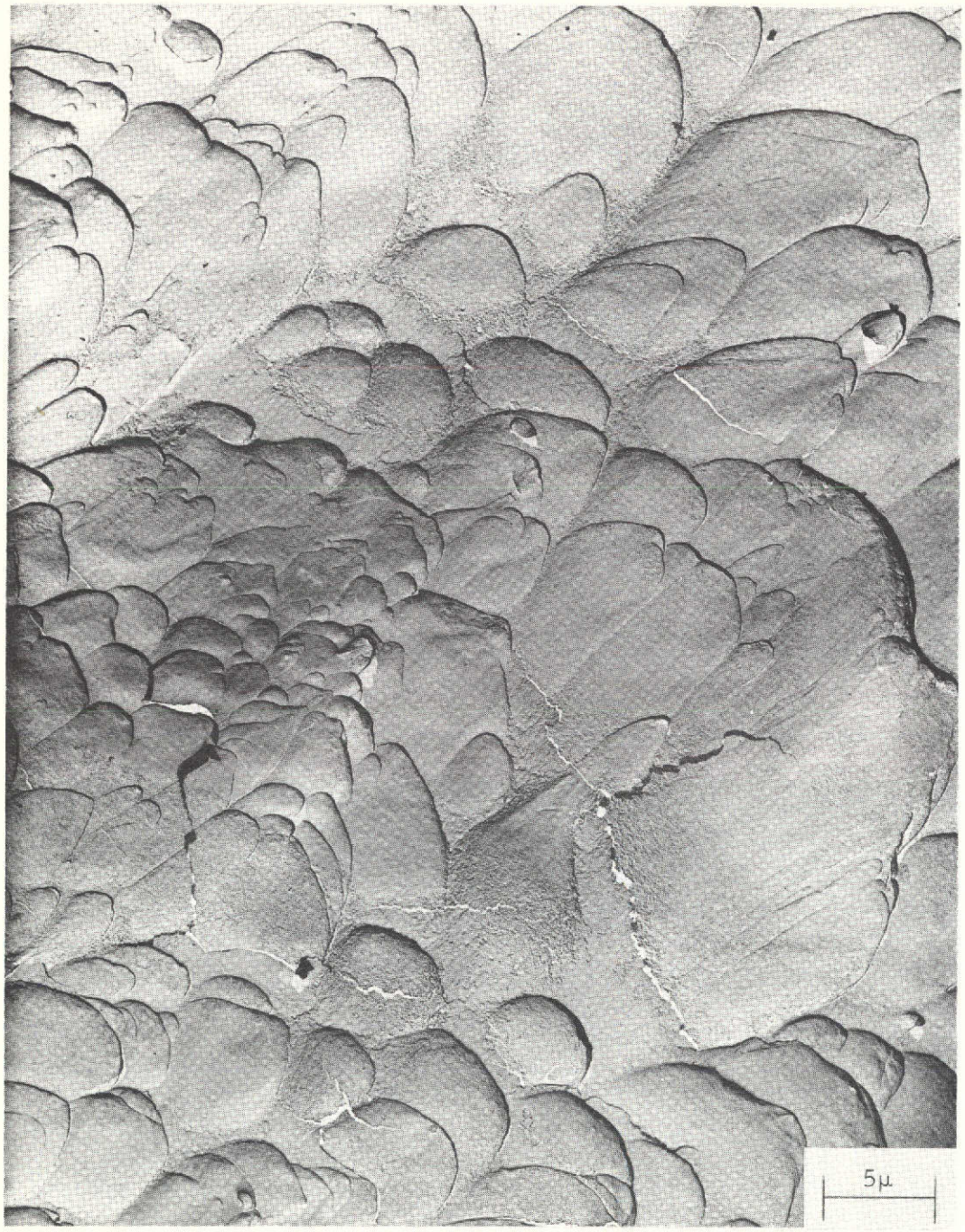

Figure 16: Fractograph of the ELI Air-Cooled Ti-5Al-2.5Sn Alloy from a Liquid Nitrogen Temperature Tensile Test.

Figure 17: Fractograph of the α-Aged Beta III Alloy from a Room Temperature Tensile Test

This page is reproduced at the back of the report by a different reproduction method to provide better detail.

SECTIONED TENSILE SAMPLES

In order to observe the microstructural features associated with the void initiation and growth stages, fractured tensile samples of these alloys were metallographically polished at their midplane. The fractured tensile samples were first coated with a 1 mil thick layer of electroless nickel using Buehler AB Edgemet. The samples were then ground to within 10 mils of the specimen midplane. During this grinding process, the specimens were oriented to reveal the plane normal to the thickness direction in the original plate. The tensile axis is in the rolling direction of the plate. The specimens were then mounted in Bakelite and ground through 320, 400, and 600 grit silicon carbide papers using automated metallographic grinding equipment. The specimens were then hand polished using 6, 3, and 1 micron diamond paste. The final polishing step was using 0.05 micron alumina powder in a vibratory polisher. There was some rounding near the edge of the samples but it did not prevent observations about the morphology of the fracture process.

To date, the sectioning of the tensile samples has been completed on the commercial air-cooled Ti-5Al-2.5Sn alloy. Both room temperature and liquid nitrogen samples have been sectioned. The specimens were etched in a HF, HNO_3, H_2O etchant with ratios of 1:3:100 to reveal the microstructure.

In the fractured room temperature samples with a plastic strain of 0.463, three different void nucleation sites were observed: twin interfaces (Figure 18a), the interface of the second phase particle (Figure 18b), and the cracking of the particle (Figure 18c). In these micrographs, the tensile axis is vertical. Most of the voids seemed to grow by slip processes rather than twinning because the voids were round and did not have linear regions which would result from twinning.

Figure 19 show the voids in the tensile sample fractured with a plastic strain of 0.304 at -320°F. Figure 19a shows a crack along a twin boundary that has no second phase particle associated with it. Figure 19b shows cracked second phase particles and Figure 19c shows a void with particles at both ends of it. Although no twin was revealed by etching, the morphology of the void in Figure 19c suggests this void formed by twinning. Most of the voids had twins associated with them which accounts for the steps which were observed on the -320°F fracture surface. From observations on a fractured sample, it is not certain if these steps are formed during the void initiation or growth stages of the fracture process.

To date, no quantitative analysis has been performed on the void nucleation or growth stages. The second phase particles which are believed to be iron-stabilized β have about the same size within any

Figure 18a

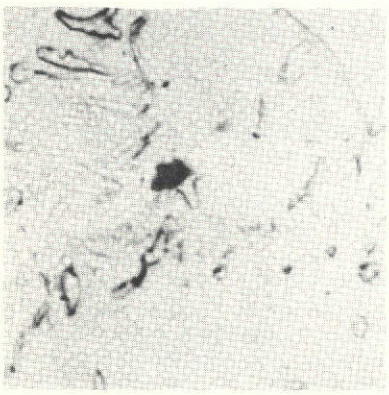

Figure 18b

Figure 18c

20μ

Figure 18: Void Initiation in a Room Temperature Tensile Test of Commercial, Air-Cooled Ti-5Al-2.5Sn by (a) Twin Interface Separation, (b) Particle-Matrix Separation, and (c) Particle Cracking.

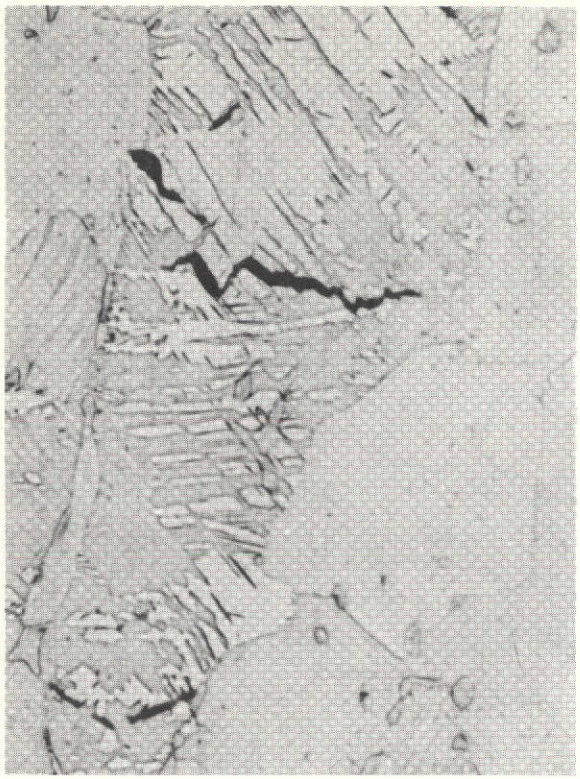

Figure 19a

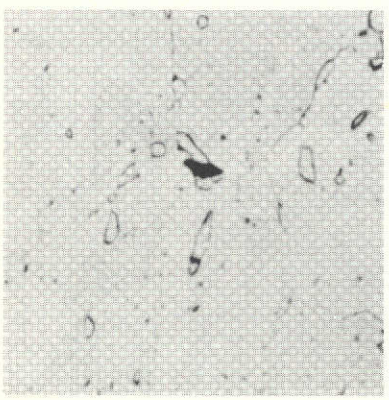

Figure 19b

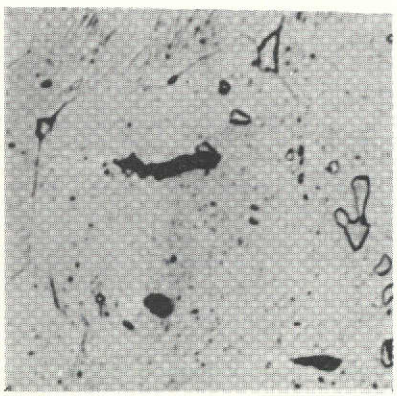

Figure 19c

20μ

Figure 19: Void Initiation in a Liquid Nitrogen Temperature Tensile Test of Commercial, Air-Cooled Ti-5Al-2.5Sn by (a) Cracking Along Twin Boundaries, (b) Cracking of Stabilized β Particles, and (c) Particles Along a Twin Crack.

Ti-5Al-2.5Sn alloy. From visual observations, it could not be determined if the particle cracking or interface separation occurred first at the larger particles in a similar fashion to the void initiation stage in aluminum alloys[1] and steels.[2]

DISCUSSION

This discussion will be limited to the Ti-5Al-2.5Sn alloys because no observations on the effect of microstructure on the fracture mechanism of Beta III have been made. As a result of observations on fractured tensile samples of the commercial, air-cooled Ti-5Al-2.5Sn alloy, the void nucleation sites are either the twin boundaries or the second phase particles which is probably iron-stabilized β.[12, 13] It is uncertain which nucleation site is responsible for the voids which result in the final rupture, because the entire deformation history cannot be observed over large regions in a fractured specimen. Twin boundaries are large two-dimensional features which have a size on the order of the materials grain size which in this case is about 50 microns. If a void is formed by failure of a particle or its interface, it will cause a stress concentration which may result in deformation by twinning. The void may then propagate along a twin boundary. On the other hand, the material may deform by twinning and nucleate voids along twin boundaries. Then particles within or close to the twinned region may fail. Nucleation of voids at particles and twin boundaries may also occur simultaneously. Observations on the midplanes of fractured tensile samples do not rule out any of these possibilities because the particle which was a nucleation site for a void which propagated along a twin or a twin which induced

the particle to crack may be above or below the plane being examined. It is very important to determine the nucleation site because each case implies a different way to effect tensile ductility through microstructural control. If twin boundaries are the nucleation sites, a reduction in grain size and minor compositional changes may be required to reduce the amount of deformation which occurs by twinning. Paton, Williams, and Rauscher[26] have shown that increasing the aluminum and oxygen content of α titanium reduces the amount of twinning present at the same strain level. If the voids are nucleated at iron-stabilized β particles, the ductility may be increased by reducing the iron content and possibly controlling the size of the particles through grain size control.

The real purpose of this investigation is to determine the effect of microstructure on fracture toughness rather than tensile ductility. In a pre-cracked specimen, such as one used for determining fracture toughness, it is possible to conceive of a situation where a crack can propagate along twin interface; while in a tensile sample, the fracture will be nucleated at the second phase particles. Thus, it becomes very important to compare the modes of fracture in cracked and uncracked samples. If the modes are identical, the nucleation stage can be studied by sectioning tensile samples which have been plastically strained to various levels short of the fracture strain. If the modes are different, a similar approach may be taken using pre-cracked or sharply notched

specimens. Amateau and Steigerwald[25] observed crack propagation by twinning in 60 mil thick high oxygen (0.30%) and low iron (0.15%) Ti-5Al-2.5Sn at -320°F. Whether this is also the case in thick sections is one of the purposes of this investigation.

In order to understand the relationship between microstructure and fracture toughness, the following work will be completed in the next stage of this investigation:

1. Tension and plane strain fracture toughness tests on Ti-5Al-2.5Sn and Beta III will be performed over the desired temperature range.
2. The fracture modes will be determined from the K_{Ic} specimen fracture surfaces.
3. The fractured K_{Ic} samples will be sectioned to compare the void nucleation sites in precracked specimens with those in tensile samples.
4. The second phase in the Ti-5Al-2.5Sn alloys will be identified using microprobe to determine the composition and X-ray diffraction to determine the crystal structure.
5. If it is determined that the fracture mode and morphology in the K_{Ic} and tensile specimens are the same, the fracture mechanism will be studied by studying several sectioned tensile samples which have been strained short of fracture. If the modes are different, the fracture process will be studied in either precracked or sharply

notched specimens using the same sectioning techniques used on the sectioned tensile samples.

CONCLUSIONS

1. The Ti-5Al-2.5Sn alloys, which are usually considered α alloys, contain a second phase which is believed to be iron-stabilized β. In the extra low interstitial level materials, which have a lower iron content, this plase has a smaller size and volume fraction.
2. The air-cooled Ti-5Al-2.5Sn alloys fail by dimpled rupture at room temperature and -320°F in tensile samples.
3. From observations on the sectioned tensile samples of air-cooled commercial Ti-5Al-2.5Sn, voids are nucleated at the second phase particle and along twin boundaries. At room temperature, the voids grow by slip processes but at liquid nitrogen temperature some void growth occurs by cracking along twin boundaries.
4. Beta III (Ti-11.5Mo-6Zr-4.5Sn) in an α-aged condition fails by dimpled rupture.
5. More work is required on both of these alloys to relate the microstructure to the fracture toughness. Work is also required to determine if observations in tension specimens is applicable to the fracture mechanism in precracked samples.

REFERENCES

1. R. H. Van Stone, R. H. Merchant, and J. R. Low, Jr., "Investigation of the Plastic Fracture of High Strength Aluminum Alloys," presented at the ASTM Low Temperature Panel Symposium, ASTM Annual Meeting, Philadelphia, June 1973.

2. T. B. Cox and J. R. Low, Jr., "An Investigation of the Plastic Fracture of High Strength Steels," NASA Technical Report No. 5, Department of Metallurgy and Materials Science, Carnegie-Mellon University, May 1973.

3. J. C. Williams, R. R. Boyer, and M. J. Blackburn, ASTM STP 453, ASTM, Philadelphia, 1969, p. 215.

4. M. A. Greenfield and H. Margolin, Met. Trans. 3, 1973, p. 2649.

5. M. J. Blackburn, Trans. AIME 239, 1967, p. 1200.

6. T. K. G. Namboodhiri, C. J. McMahon, Jr., and H. Herman, Met. Trans. 4, 1973, p. 1323.

7. D. J. Truax and C. J. McMahon, Jr., Corrosion, 1972, p. 47.

8. M. J. Blackburn and J. C. Williams, Trans. ASM 62, 1969, p. 398.

9. H. Conrad, K. Okasaki, V. Gadgil, and M. Jon, Electron Microscopy and Structure of Materials, Gareth Thomas, Editor, University of California Press, Berkeley, 1972, p. 438.

10. J. L. Shannon, Jr. and W. F. Brown, Jr., Proc. ASTM 63, 1963, p. 809.

11. E. F. Erbin, Proc. ASTM 63, 1963, p. 826.

12. J. L. Christian, A. Hurlich, J. E. Chafey, and J. F. Watson, Proc. ASTM 63, 1963, p. 578.

13. R. E. Curtis, R. R. Boyer, and J. C. Williams, Trans. ASM 62, 1969, p. 457.

14. J. C. Williams, B. S. Hickman, and H. L. Marcus, Met. Trans. 2, 1971, p. 1913.

15. J. C. Williams, B. S. Hickman, D. H. Leslie, Met. Trans. 2, 1971, p. 477.

16. F. H. Froes, J. M. Capenos, and M. G. H. Wells, Titanium Science and Technology, R. I. Jaffee and H. M. Burte, Editors, Plenum Press, New York, 1973, p. 1621.

17. V. C. Petersen, F. H. Froes, and R. F. Malone, Titanium Science and Technology, 1973, p. 1969.

18. J. A. Feeney and M. J. Blackburn, Met. Trans. 1, 1970, p. 3309.

19. J. B. Guernsey, V. C. Petersen, and F. H. Froes, Met. Trans. 3, 1972, p. 339.

20. F. H. Froes, Private Communication.

21. ASTM Standard E399-72, Annual Book of ASTM Standards, Part 31, 1972, p. 955.

22. J. L. Shannon, Jr., Private Communication.

23. George E. Dieter, Jr., Mechanical Metallurgy, McGraw-Hill, New York, 1961, p. 237.

24. P. W. Bridgman, Studies in Large Plastic Flow and Fracture, McGraw-Hill, New York, 1952, p. 9.

25. M. F. Amateau and F. A. Steigerwald, "The Relationship Between Plastic Deformation and Fracture in Alpha Titanium" AFML-TR-66-263, June 1966.

26. N. E. Paton, J. C. Williams, and G. P. Rauscher, Titanium Science and Technology, R. I. Jaffee and H. M. Burte, Editors, Plenum Press, 1973, p. 1049.

27. Max Hansen, Constitution of Binary Alloys, McGraw-Hill, New York, 1958, p. 1210.

THE FOLLOWING PAGES ARE DUPLICATES OF ILLUSTRATIONS APPEARING ELSEWHERE IN THIS REPORT. THEY HAVE BEEN REPRODUCED HERE BY A DIFFERENT METHOD TO PROVIDE BETTER DETAIL